Supporting Information for:

Shape Control of Silver Nanoparticles and Their Stability on Al_2O_3

Graham C. Beaton[1], Adam J. Bottomley[1], Daniel Prezgot[2], Anatoli Ianoul[2], and Kevin G. Stamplecoskie*[1]

[1]Queen's University Department of Chemistry, Chernoff Hall, 90 Bader Ln. Kingston, Ontario, CA

[2]Carelton University Department of Chemistry 227 Steacie building, 1125 Colonel dr. Ottawa, Ontario, CA

Experimental

α-Terpineol, ethyl cellulose, Al_2O_3 nanoparticles, $AgNO_3$, sodium citrate dihydrate and $NaBH_4$ were purchased from Sigma Aldrich and. Benzyl Alcohol was purchased from BDH Chemical Co. These reagents were used without further purification.

Aluminum oxide resign was synthesized through addition of α-Terpineol (27.27 mmol) with benzyl alcohol (7.212 mmol) to a dry scintillation vial and stirred moderately until homogeneous. The solution was then heated to 70℃ and maintained stirring with slow addition of ethyl cellulose (0.55 mmol) and stirred until full solubility of ethyl cellulose was achieved. While maintaining temperature, aluminum oxide nanoparticles (>50 nm, 20% Wt. Solution in Isopropanol, 2.5 mL) were added and solution was left to stir for 30 minutes. Resulting solution was a viscous white liquid free of particulates.

Alumina supported AgNP colloids were synthesized by first solubilizing Al_2O_3 nanoparticles in trace amounts of isopropanol and water, adding desired weight % Ag precursor in the form of $AgNO_3$ and performing a drop wise addition of equal molar concentration $NaBH_4$ (aq.) at a rate of 1 mL / minute. All under constant magnetic stirring ~ 700 rpm. Reduction and formation of final particles were complete within 10 minutes of adding reductant.

AgNP substrates were grown onto 1 square inch borosilicate microscope slides, spin coated with aluminum oxide paste at 6000 RPM. Following the spin coat of alumina paste, films were heated to 80℃ for 1 hour to evaporate the solvent left over from spin coating and subsequently heated at 500℃ in a muffle furnace for 1 hour to remove hydrocarbons bonded to the film surface in preparation for SILAR. Successive ion layer adsorption reactions were used to grow the initial SILAR particles by submerging alumina treated slides in aqueous solution of $AgNO_3$ (10 mM), rinsing with Mili-Q DI water and submerging in aqueous solution of $NaBH_4$ (10 mM). AgNO3 acts as a silver ion source while NaBH4 serves as a reducing agent for the initial and subsequent deposition of silver. This process was repeated until ideal layer concentrations were achieved.

Photochemical shape control reactions were performed on 15 layer SILAR AgNP films and varying weight % Ag loaded colloids, in aqueous sodium citrate dihydrate solution (4.0 mM), with 16 hour irradiation durations for each wavelength used. Thin films were irradiated with LuzChem^{TM} Photoilluminator with 455 nm, 525 nm and 625 nm LED heads. Power and wavelength information for LEDs used are summarized in Table S2 of this document.

Numerical Modelling. Finite difference time domain modelling was performed using Lumerical Solutions Inc. (FDTD Solutions v8.17. An 800 nm cubic simulation space was used with a perfect matched layer (PML) boundary (12 layers). A total-field scattered-field (TFSF) light source was used, absorption and scattering cross sections were measured from power transmission monitors in the scattered field and total field areas respectively. Extinction was calculated as the sum of absorption and scattering cross sections. Frequency-domain field profile monitors were used to calculate E/E_0. A non-uniform mesh was used, with a mesh override region containing a 0.5 nm mesh size extended at least 10 nm past the nanostructures. All dielectric-dielectric and metal-dielectric boundaries were treated with Lumerical's Conformal Mesh Technology (CMT), a proprietary extension of the Yu-Mittra method.[1] The material was described by an analytical model fitted to tabulated permittivity data of silver.[2] The simulation objects consisted of: triangular prisms with an edge length of 45 – 95 nm, a thickness of 14 nm and a corner radius of 15% their edge length in a background index if $n = 1$; rounded decahedra with edge lengths of 30 – 70 nm and a corner radius of 5 nm in a background index of $n = 1.33$ to represent the SILAR particles more heavily imbedded in the alumina matrix.

(1) Yu, W.; Mittra, R. A Conformal Finite Difference Time Domain Technique for Modeling Curved Dielectric Surfaces. *IEEE Microw. Wirel. Components Lett.* **2001**, *11* (1), 25–27.

(2) Palik, E. D. *Handbook of Optical Constants of Solids*; 1985; Vol. 1.

Instrumentation

UV−Vis absorption spectra of the substrates were acquired with a Varian Cary 60 UV-Vis spectrophotometer, scanning from 900-300 nm.

Transmission electron microscopy images were acquired and characterized with a FEI Osiris S/TEM operated at 200 keV. The microscope is equipped with an FEI ChemiSTEM^{TM} system, comprising of four energy-dispersive X-ray spectroscopy (EDS) detectors in close proximity to the sample.

Bright-field TEM images were taken with a probe current of 2.8 nA and both high-angle annular dark-field (HAADF) images and spectral imaging were carried out with a probe current of 0.6 nA

The XPS spectra were measured on a Kratos AXIS Nova spectrometer equipped with an Al X-ray source. Each sample was mounted onto a coated aluminum platen using double-sided adhesive Cu tape and was kept under high vacuum (10^{-8} Torr) overnight inside the preparation chamber before they were transferred into the analysis chamber (ultrahigh vacuum, 10^{-9} Torr) of the spectrometer.

The XPS data were collected using AlK_{α} radiation at 1486.69 eV (150 W, 10 mA), charge neutralizer and a delay-line detector (DLD) consisting of three multi-channel plates. Binding energies are referred to the C1s peak at 285 eV. Survey spectra were recorded from -5 to 1200 eV at a pass energy of 160 eV (number of sweeps: 2) using an energy step size of 1 eV and a dwell time of 100 ms. High resolution spectra for O1s, Ti2p, Ag3d, C1s, Si2p and Al2p were recorded in the appropriate regions at a pass energy of 20 eV (number of sweeps: O1s, 5; Ti2p, 15; Ag3d, 10; C1s, 10; Si2p, 10; Al2p, 10) using a dwell time of 300 ms and an energy step size of 0.1 eV. The analyzed area on the specimens was about 300 × 700 mm^2 (lens mode: FOV 1) at this position. The incident angle (X-ray source/sample) is the magic angle of 54.74° and the take-off angle (sample/detector) is 90°.

The spectra were measured using the *ESCApe* software [1] and converted to *.vms files for using the *CasaXPS* software [2]. The XPS data were processed using the *CasaXPS* software [2]. The data were corrected for energy shifts due to charging of the sample under the influence of the X-rays and the spectra were corrected for background using the Shirley (HiRes scans) algorithm. Peak fits were obtained using symmetric {Gaussian-Lorentzian – GL(30)} and asymmetric lineshapes (LA).

Figure S1 (a) XPS data for Silica supported AgNP

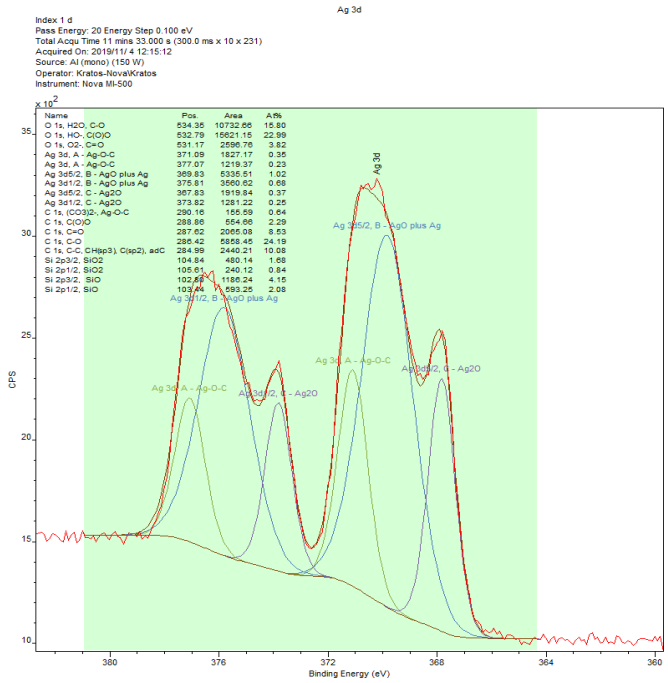

Figure S1(b) XPS data for Titania supported AgNP

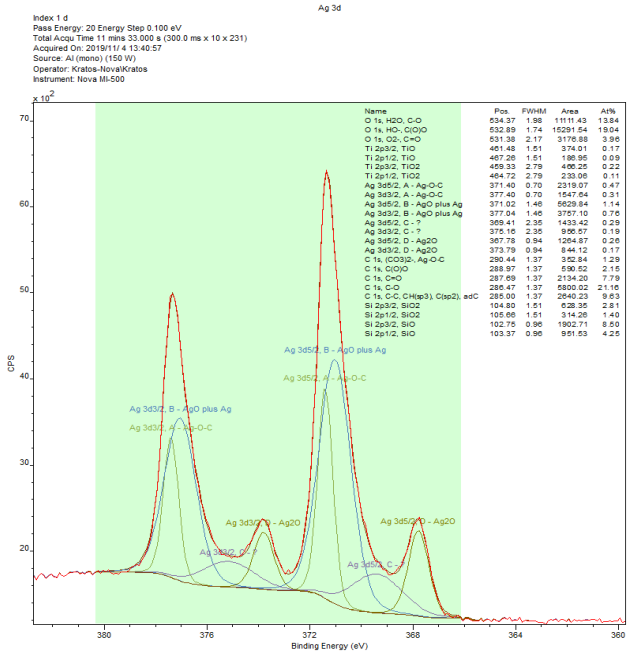

Figure S1 (c) XPS data for Alumina supported AgNP

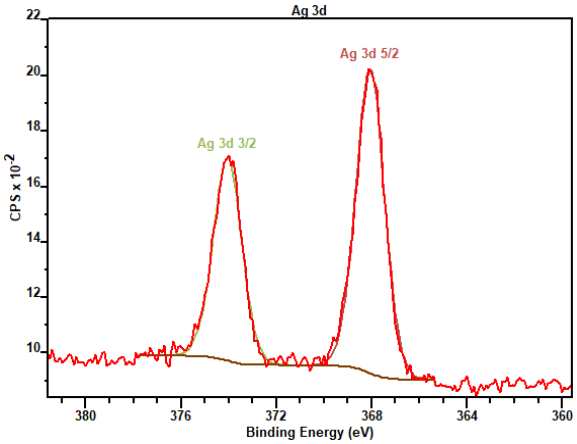

Figure S1 (d) XPS data for Non-supported AgNP

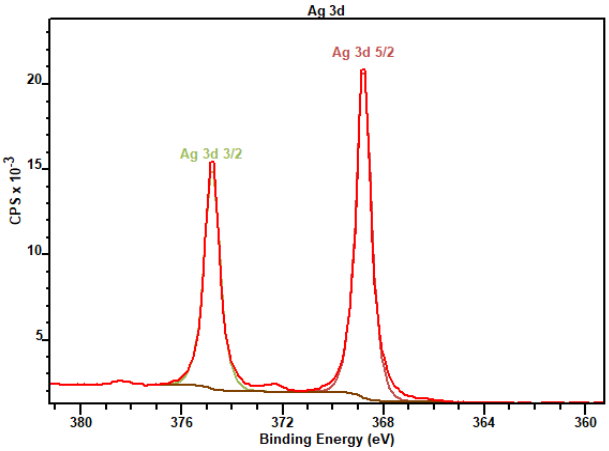

Figure S2: Absorbance spectra of alumina colloid supported AgNP before and after 60 days of exposure to air and overhead lighting. Solvent was fully evaporated, and particles were re-suspended in aqueous solution.

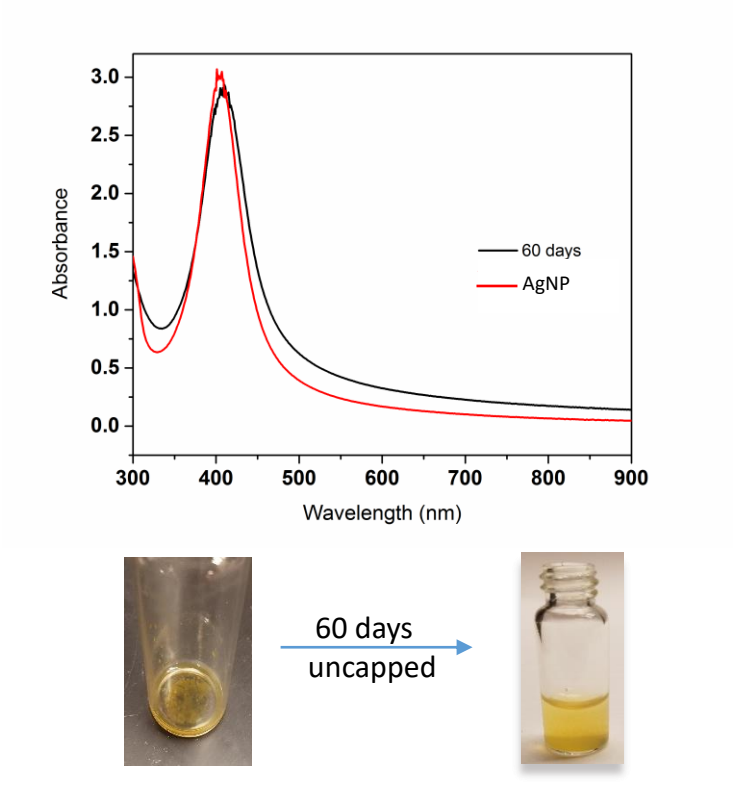

Figure S3(a): Absorbance spectra of alumina colloid supported AgNP synthesized with increasing wt. % loading of Ag precursor.

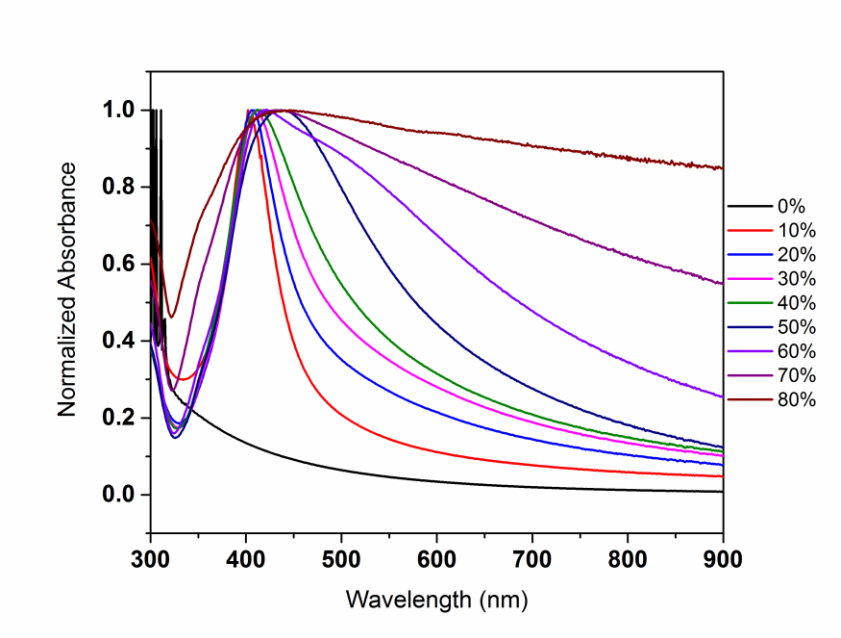

Figure S3(b): TEM particle diameter histogram for 20 particles synthesized at 10 wt% Ag and 20 synthesized with 50 wt% Ag in the presence of colloidal Al_2O_3

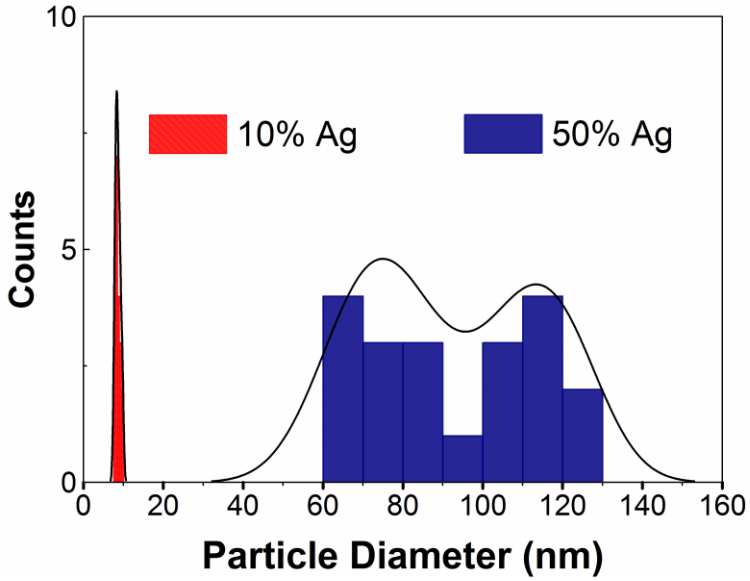

Table S1: Plasmon absorbance data for alumina colloid supported AgNP synthesized with increasing wt. % loading of Ag precursor

% Wt. Ag	Plasmon absorbance maximum (nm)	Full Width at Half Maximum (nm)
10	402	78
20	407	80
30	410	99
40	416	123
50	441	174
60	441	223
70	441	N/A
80	441	N/A

Figure S4: Absorbance spectra of alumina supported AgNP thin films grown with increasing SILAR reaction cycles

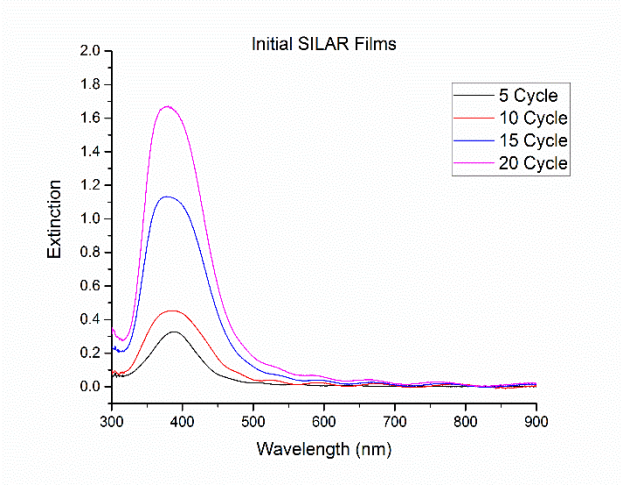

Table S2: Luzchem LED photoilluminator specs used for photochemical synthesis of all AgNP products

LED Color	Wavelength (centered) (nm)	FWHM (nm)	Irradiance (W/m^2)
Blue	455	25	25,400
Green	525	46	6,810

Red	625	23	10,930

Figure S5: HAADF (a) and EDX chemical mapping (b) images of initial SILAR ~8nm, spherical AgNP substrate films. Particles were sonicated to remove them from the film and suspended on a Cu TEM grid for imaging.

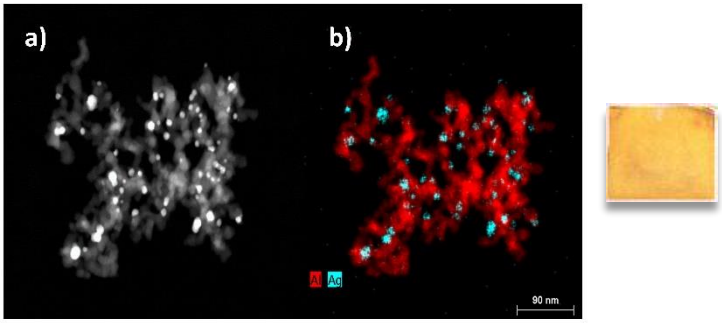

Dark-field imaging and chemical mapping shows the incorporation of Ag in the alumina scaffolding. Brightest spots in this image which correspond to the darkest spots in the reported bright-field TEM imaging represent the AgNP. This is confirmed with Chemical mapping where the Ag is mapped in light blue and the Al is mapped in red.

Figure S6: Atomic force microscopy phase imaging for an aluminum oxide coated microscope slide (a) and 625 nm LED AgNP photo-product (b).

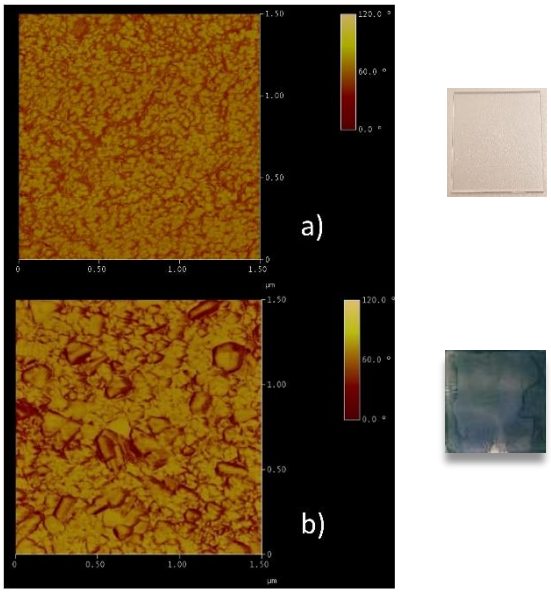

AFM imaging for alumina films and AgNP photoproduct film shows the nature in which the AgNP plates are embedded and arranged within the alumina scaffold layer. This imaging proves the AgNP do not all align themselves on one face or edge of the particle but grow in many directions within the scaffolding.

Image S1: Alumina colloid supported AgNP photoproducts. From left to right: Initial seeds, 455 nm, 525 nm and 625 nm products.

Image S2: Alumina solid supported AgNP thin-film photoproducts.

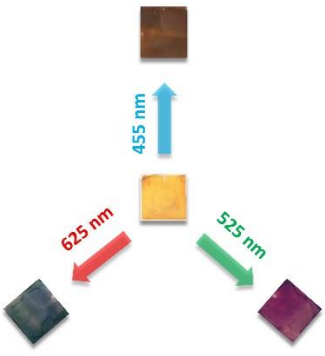

Figure S8: Absorbance spectra of alumina supported AgNP colloid heated at 80 °C for 3 hours

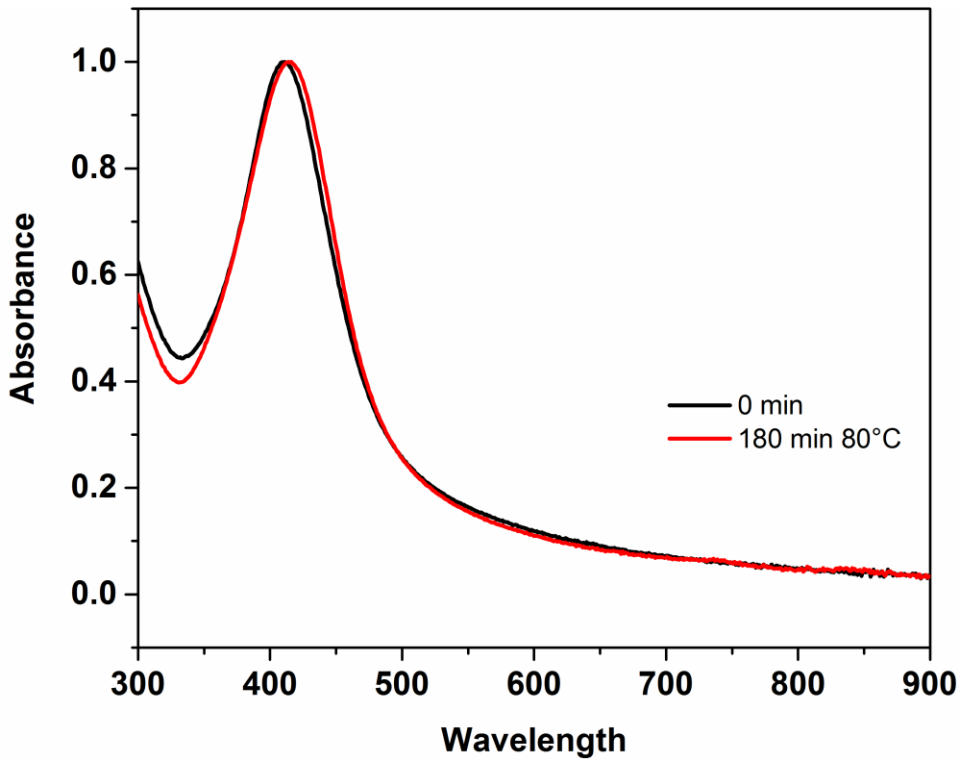

Alumina supported 5 wt% Ag colloidal AgNP was subjected to heating at 80°C for 3 hours with no changes to the absorbance features after this time. This stability further suggests its potential use in catalysis where increased reaction temperature is often needed.

Figure S9: Extinction cross-section calculated for trigonal plates 45 and 55 nm in edge length vs experimental 525 nm LED photo-product

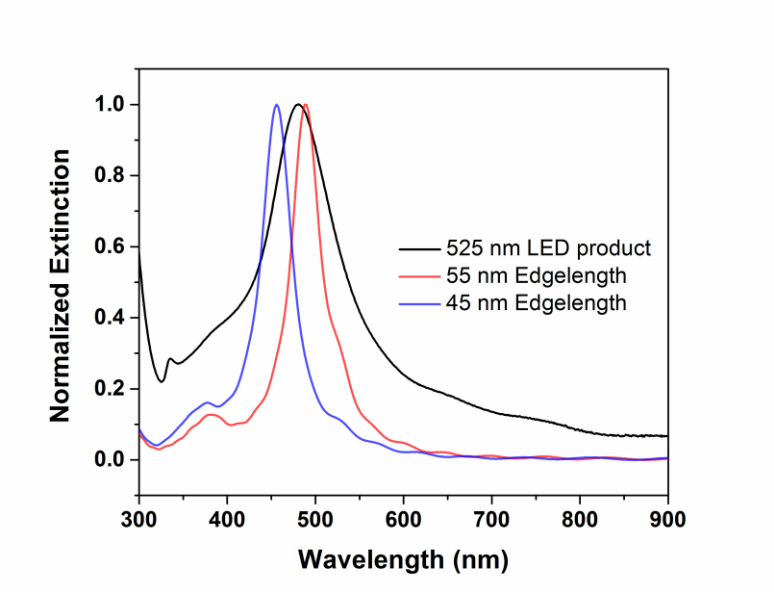

Figure S10: Extinction cross-section calculated for decahedra increasing in edge length

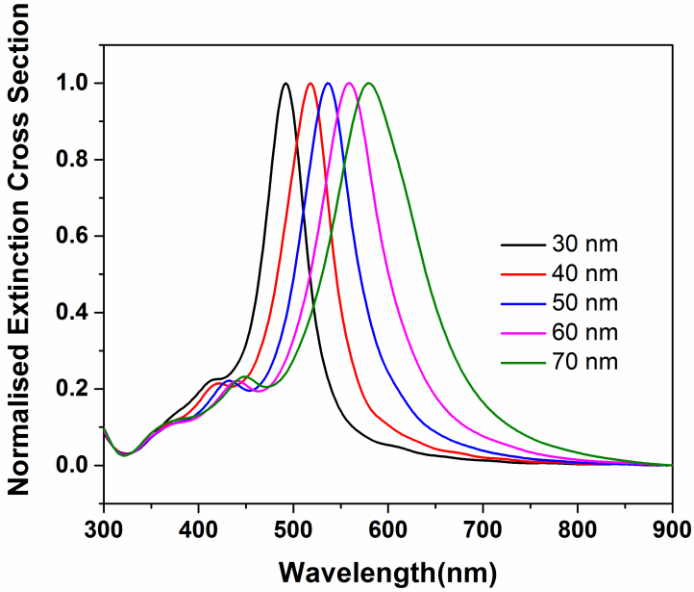

Figure S11: Extinction cross-section calculated for hexagonal plates increasing in edge length

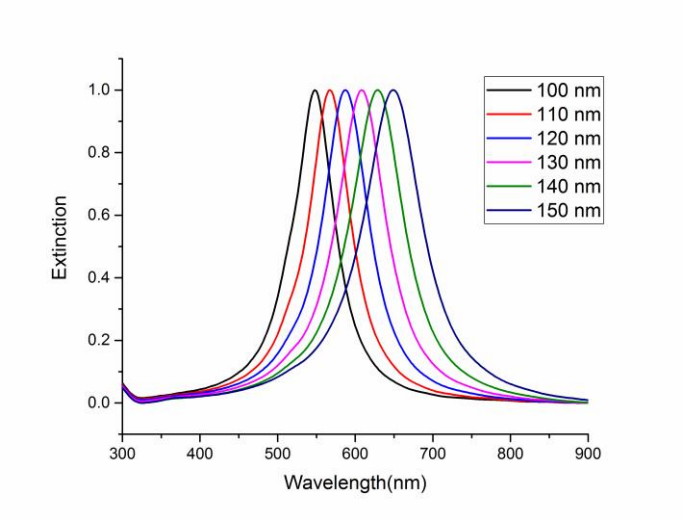

Figure S12: Extinction cross-section calculated for trigonal plates increasing in edge length

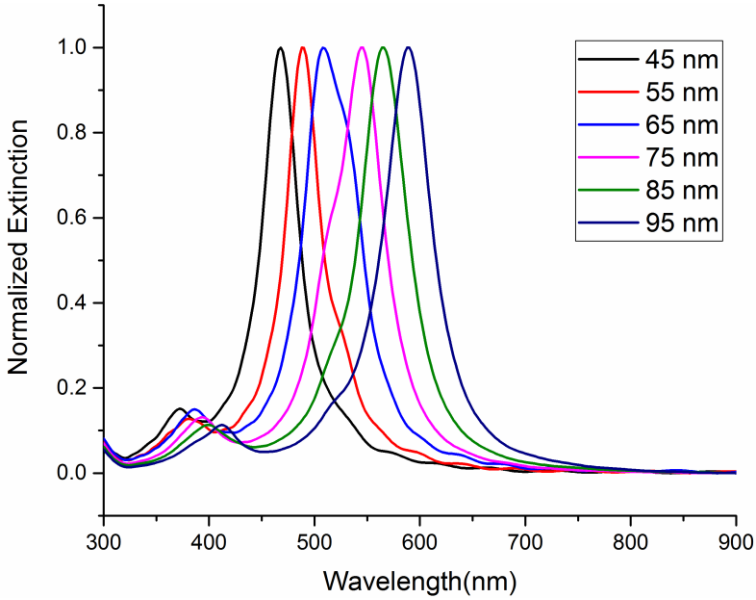

Figure S13: Extinction cross-section for colloid AgNP photo-product simulations and their calculated local electronic field enhancement excited at 455 nm (A) 525 nm (B) and 625 nm (C).

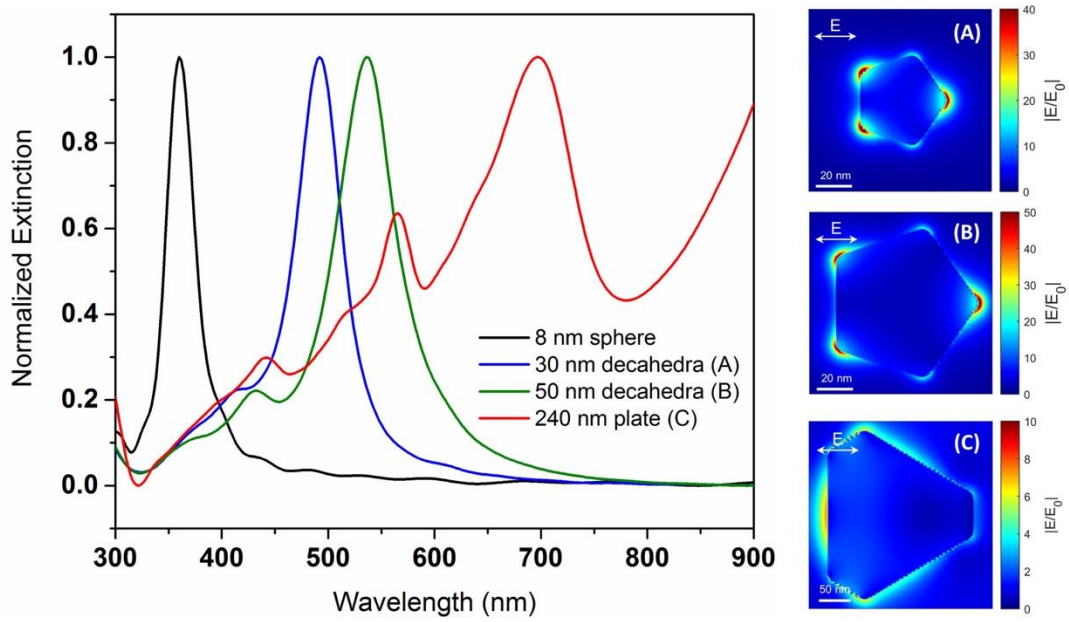

Figure S14: Extinction cross-section for solid thin filmAgNP photo-product simulations and their calculated local electronic field enhancement excited at 455 nm (A) 525 nm (B) and 625 nm (C).

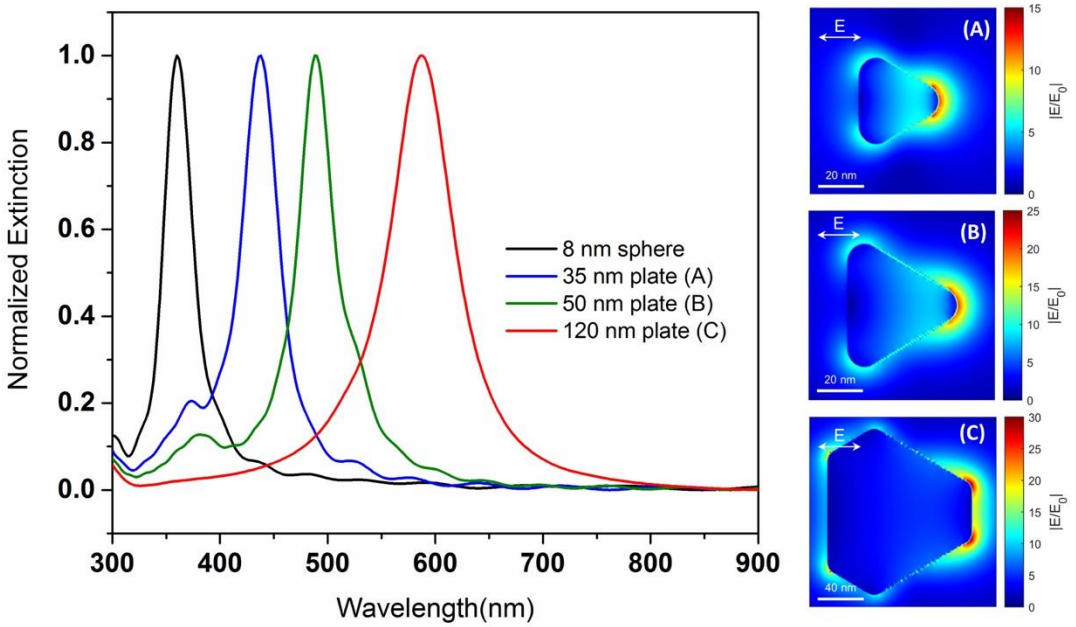

Figure S15: Activation mechanism for the concerted oxidation of citrate and reduction of AgNP surfaces, leaving them labile to photochemical shape control

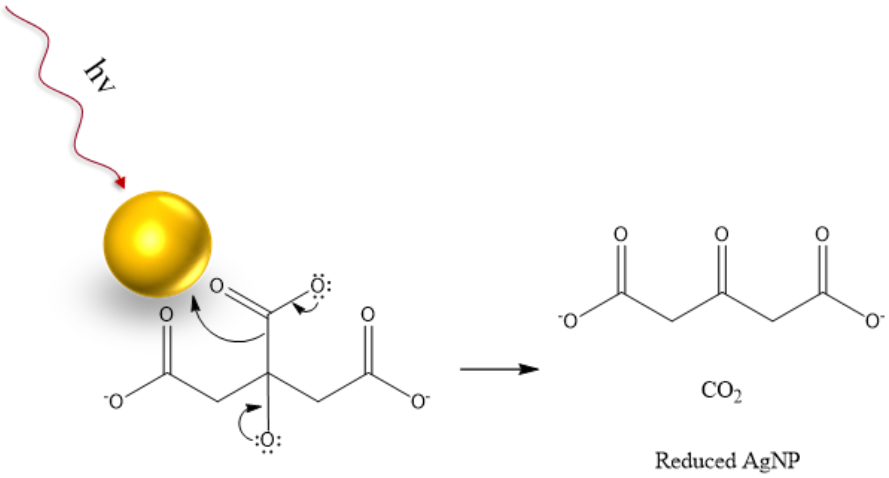

Figure S16: 455 nm colloid product

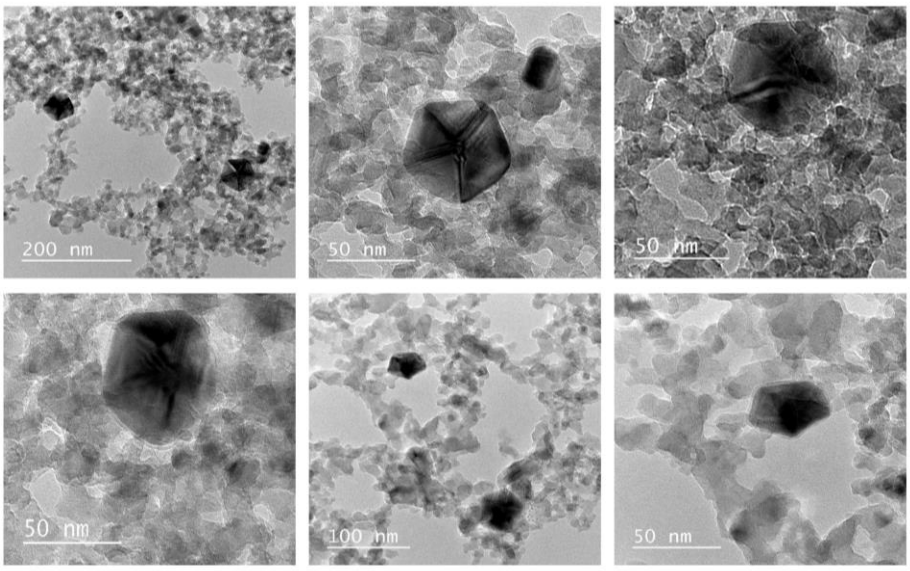

Figure S17: 525 nm colloid product

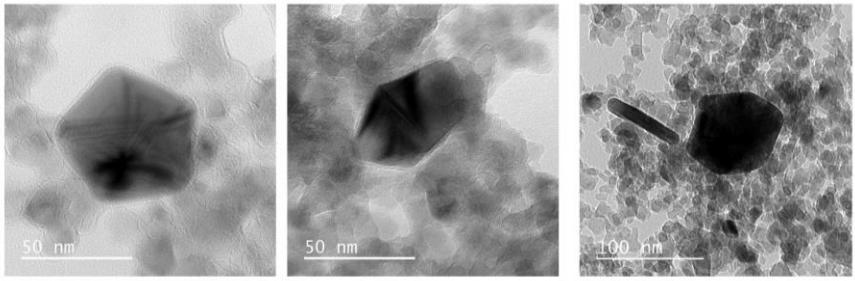

Figure S18: 625 nm colloid product

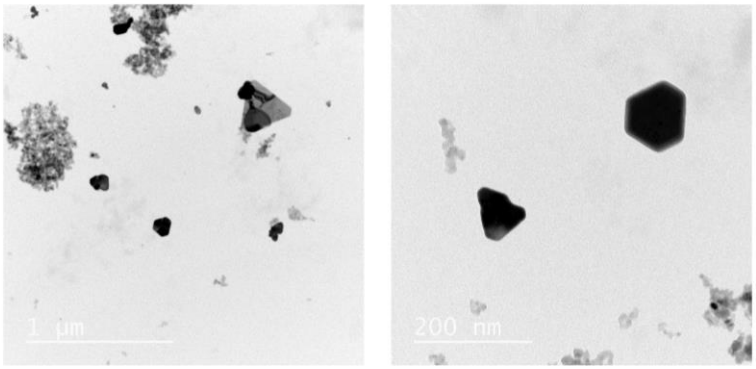

Figure S19: 455 nm thin-film product

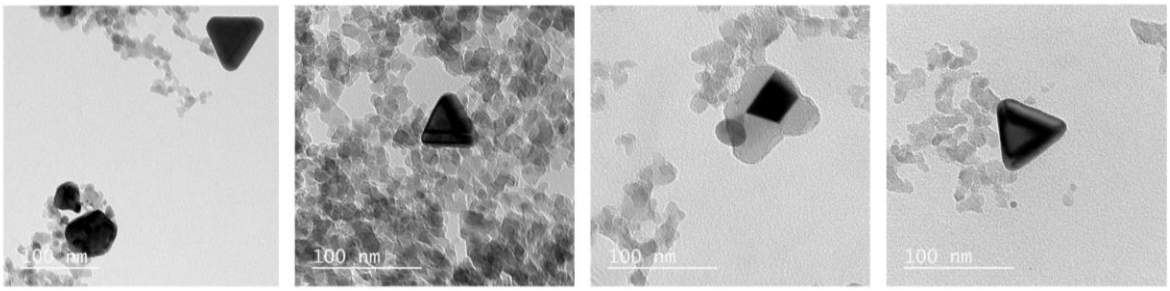

Figure S20: 525 nm thin-film product

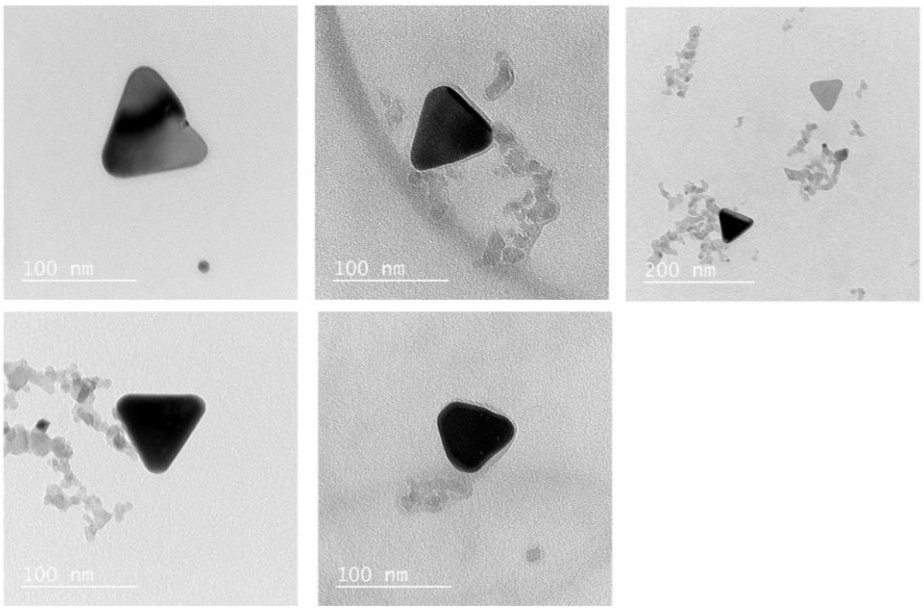

Figure 21: 625 nm thin-film product

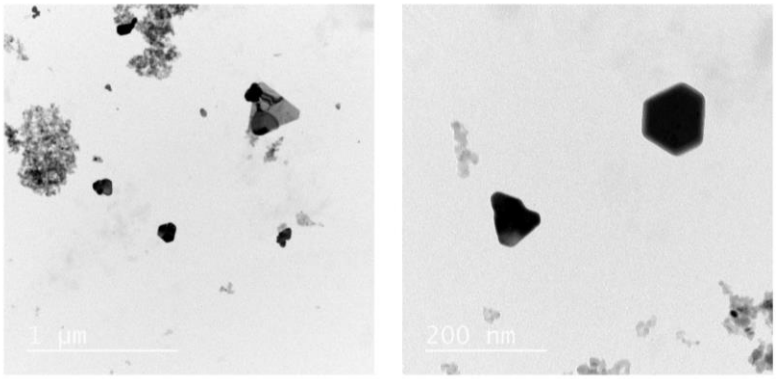

Figure S22: Calculated extinction cross-section of 50 nm edge length decahedra AgNP, with individual component contributions of scattering and absorbance calculated and plotted.

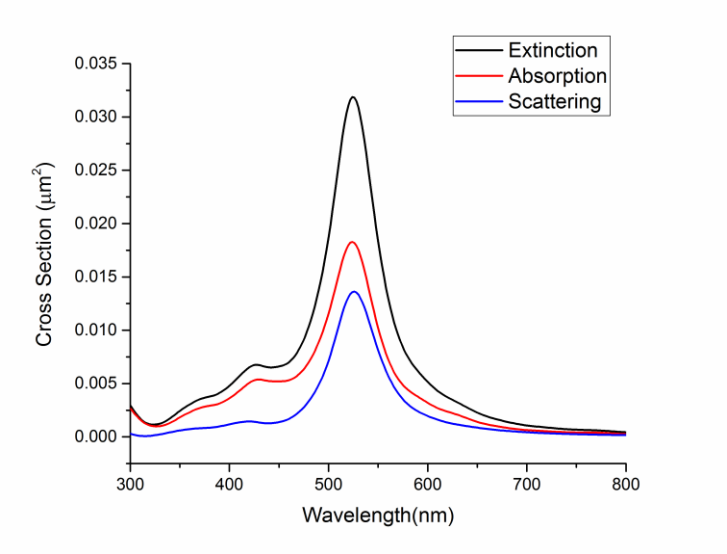
Extinction
Absorption
Scattering
Cross Section (μm²)
0.035
0.030
0.025
0.020
0.015
0.010
0.005
0.000
300
400
500
600
700
800
Wavelength(nm)